Two Elastodynamic Incremental Models: The Incremental Theory of Diffraction and a Huygens Method

Michel Darmon, Audrey Kamta Djakou, Samar Chehade, Catherine Potel, Larissa Fradkin

Two elastodynamic incremental models: the Incremental Theory of Diffraction (ITD) and a Huygens method

M. Darmon, A. Kamta Djakou, S. Chehade, C. Potel and L. Fradkin

***Abstract*— The elastodynamic Geometrical Theory of Diffraction (GTD) has proved to be useful in ultrasonic Non-Destructive Testing (NDT) and utilizes the so-called diffraction coefficients obtained by solving canonical problems, such as diffraction from a half-plane or an infinite wedge. Consequently applying GTD as a ray method leads to several limitations notably when the scatterer contour cannot be locally approximated by a straight infinite line: when the contour has a singularity (for instance at a corner of a rectangular scatterer), the GTD field is therefore spatially non-uniform. In particular, defects encountered in ultrasonic NDT have contours of complex shape and finite length. Incremental models represent an alternative to standard GTD in the view of overcoming its limitations. Two elastodynamic incremental models have been developed to better take into consideration the finite length and shape of the defect contour and provide a more physical representation of the edge diffracted field: the first one is an extension to elastodynamics of the Incremental Theory of Diffraction (ITD) previously developed in electromagnetism while the second one relies on the Huygens principle. These two methods have been tested numerically, showing that they predict a spatially continuous scattered field and their experimental validation is presented in a 3D configuration.**

***Index Terms*—Elastodynamics, GTD, incremental models, ITD, Huygens**

I. Introduction

THE scattering of elastic waves from defects is of great interest in ultrasonic Non-Destructive Testing (NDT). The Geometrical Theory of Diffraction (GTD) is a classical method used for modelling diffraction from cracks, which behave locally as half-planes or infinite wedges [1], [2]. It is a high frequency ray method, which in addition to incident and reflected rays, introduces diffracted rays and describes the diffracted field they carry using the diffraction coefficients calculated for half-planes or infinite wedges, respectively. In other words, GTD relies on the locality principle of high frequency phenomena, which stipulates that if the vicinity of each diffraction point along the obstacle contour can be described, maybe approximately, by an infinite tangent half-plane or by an infinite planar wedge, then the diffracted field radiated by this point can be described using the corresponding GTD diffraction coefficients. However, in ultrasonic NDT it is not uncommon to encounter a diffracting edge of a flaw that cannot be approximated, even locally, by a straight line or planar wedge: as shown in next Figs. 3a) and 4a). GTD produces a discontinuity at the shadow boundaries emanating from the edge endpoints (for instance a corner of a rectangular defect) since the GTD field is null out of the diffraction cone. GTD has other drawbacks of ray tracing: searching for the diffraction point for each observation point is not so straightforward in complex 3D configurations and the GTD invalidity at caustics requires a uniform correction using special functions [3].

Incremental methods have been developed, originally in electromagnetism, to overcome these GTD limitations: Incremental Theory of Diffraction (ITD) [4]–[6], Incremental Length Diffraction Coefficient (ILDC) [7] and Equivalent Edge Currents (EEC) [8]. Unlike GTD, incremental methods do not require ray tracing. They treat points of the diffracting edge as fictitious sources of the field called incremental field, and the scattered field at an observation point is calculated as the sum of these incremental contributions. Incremental models provide an extension for observation angles outside of the diffraction cone and a natural uniform representation of the scattered field at caustics [4] or at the shadow boundaries emanating from edge endpoints. Incremental methods are particularly useful to better take into account the finite length and shape of a defect contour. To model diffraction from an edge of finite size, ITD can be based on GTD or [5] UTD (Uniform Theory of Diffraction [9]), UTD being a GTD uniform correction, valid inside penumbras of incident or reflected rays and outside [9].

As in ultrasonic NDT, a crack is usually no more than a few centimeters long [10], inspections are carried out at high frequency (1 – 10 MHz). GTD can be utilized, because cracks are usually large compared to the corresponding wavelengths. But GTD is theoretically valid for an infinite edge and modelling has to take into account the crack's finite extent.

This paper aims at developing elastodynamic incremental

Submitted on February 11, 2019.

M. Darmon (e-mail: michel.darmon@cea.fr), and S. Chehade (e-mail: samar.chehade@cea.fr) are at CEA LIST, Department of Imaging and Simulation for Nondestructive Testing, 91191 Gif-Sur-Yvette, France (FR). They are also at E.D. EOBE, University Paris-Saclay (FR).

A. Kamta Djakou (e-mail: noelleaudrey@gmail.com) is also at CEA LIST.

C. Potel (e-mail: catherine.potel@univ-lemans.fr) is at Fédération Acoustique du Nord Ouest (FANO), CNRS 3110, FR, and at Laboratoire d'Acoustique de l'Université du Maine (LAUM), UMR CNRS 6613, 72085 Le Mans cedex 9, FR.

L. Fradkin (e-mail: l.fradkin@soundmathematics.com) is at Sound Mathematics Ltd., Cambridge CB4 2AS, UK

models for isotropic solids, with application to ultrasonic NDT. An elastodynamic incremental model was developed before for an elliptical crack [11]: it is based on a Kirchhoff approximation integral on a line and will consequently necessarily predict erroneous amplitudes of edge diffracted fields; that's why the elastodynamic Kirchhoff prediction has been improved using the Physical Theory of Diffraction (PTD) [12] especially for shear waves [12].

The methods proposed in the current paper are more effective than this Kirchhoff-based method [11] since they rely on GTD or PTD which is a much better recipe than Kirchhoff for modelling edge diffraction. In section II, an elastodynamic ITD is developed using the standard approach previously developed in electromagnetism [4]. A new elastodynamic incremental model based on the Huygens principle is also proposed. Section III describes numerical and experimental validations of both models. Section IV offers conclusions.

II. Incremental models

Let us consider a curved stress-fee crack of contour $\mathcal{L}$ embedded in an elastic homogeneous and isotropic space. Let the crack be irradiated by a plane wave (Fig. 1)

$$\mathbf{u}^{\boldsymbol{\alpha}}(\mathbf{x}) = A\,\mathbf{d}^{\alpha} e^{i(-\omega t + \mathbf{k}^{\alpha}\cdot\,\mathbf{x})}, \tag{1}$$

where the superscript $\alpha = $ L, TV or TH (Longitudinal, Transverse Vertical or Transverse Horizontal) is used to denote the incident wave mode, A is the wave amplitude, $\mathbf{d}^{\alpha}$ its polarization (unit vector in the direction of particle motion), $\mathbf{k}^{\alpha}$ its wave vector whose magnitude is noted $k_\alpha = \omega/c_\alpha$, with ω the circular frequency and c_α the speed of the corresponding mode, i the imaginary unit, t is time and $\mathbf{x}$ is the observation point. Below the exponential factor $\exp(-i\omega t)$ is implied but omitted everywhere.

Incremental methods assume that points Q_l of the diffracting edge are all fictitious Huygens sources of a field defined as the incremental field $\boldsymbol{F}_\beta(Q_l, \mathbf{x})$. Then at an observation point $\mathbf{x}$ the field $\boldsymbol{v}_\beta$ diffracted by the contour $\mathcal{L}$ is the integral over the contour $\mathcal{L}$ of the incremental field:

$$\boldsymbol{v}_\beta^{\alpha}(\mathbf{x}) = \int_{\mathcal{L}} \boldsymbol{F}_\beta(Q_l, \mathbf{x})\; e^{ik_\alpha\, l\cos\Omega_\alpha(l)} dl\,, \tag{2}$$

with dl being the edge increment. We have developed two different methods to determine this incremental field in elastodynamics: one based on the GTD locality principle (ITD) and one based on the Huygens principle.

A. Elastodynamic Incremental Theory of Diffraction (ITD)

At the diffraction point Q_l, let the crack edge be approximated by a half-plane tangent to the edge at this diffraction point (see Fig. 1). Let Q_l be the origin of the local Cartesian coordinate system $\{\mathbf{e}'_x, \mathbf{e}'_y, \mathbf{e}'_z\}$ associated with this half-plane. It is convenient to express the incident wave vector $\mathbf{k}^{\boldsymbol{\alpha}} = k_\alpha.(\sin\Omega_\alpha\cos\theta_\alpha, \sin\Omega_\alpha\sin\theta_\alpha, \cos\Omega_\alpha)$ in the associated spherical coordinates $(k_\alpha, \Omega_\alpha, \theta_\alpha)$ and the observation point $\mathbf{x}$, using either the local Cartesian coordinates (x', y', z') or another set of associated local spherical coordinates (s', ϕ, θ).

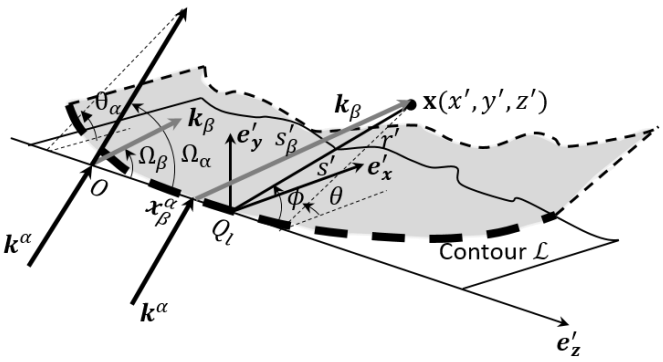

Fig. 1. A plane wave with the propagation vector $\boldsymbol{k}^{\boldsymbol{\alpha}}$ incident on a stress-free crack (in gray) of contour $\mathcal{L}$. Thick black arrow – direction of the incident wave; thick gray arrow - direction of the wave scattered by the half-plane tangent to the crack at the diffraction point Q_l.

The exact scattered field $\boldsymbol{u}_\beta^\alpha(\mathbf{x}, \Omega_\alpha, \theta_\alpha)$ generated by a plane elastic wave irradiating a half-plane can be described using the plane wave spectral decomposition [2]:

$$\boldsymbol{u}_\beta^\alpha(\mathbf{x}, \Omega_\alpha, \theta_\alpha) = i\frac{q_\beta \kappa_\beta}{2\pi}\int_\Gamma \Psi_\beta(\lambda, \Omega_\alpha, \theta_\alpha)\sin\lambda\, \boldsymbol{d}_{\boldsymbol{\beta}}(\Omega_\beta, \theta) \\ e^{ik_\beta[r'\sin\Omega_\beta\cos(\lambda-\bar{\theta}) + z'\cos\Omega_\beta]} d\lambda, \tag{3}$$

with β denoting the scattered wave mode, $q_\beta = k_\beta\sin\Omega_\beta$, $\kappa_\beta = c_L/c_\beta$ the dimensionless slowness of the scattered wave,

$$\Psi_\beta\big(-q_\beta\cos\lambda, sgn(\sin\theta)\big) = \frac{\mathrm{g}_\beta(-q_\beta\cos\lambda, sgn(\sin\theta))}{q_\alpha\cos\theta_\alpha - q_\beta\cos\lambda}, \tag{4}$$

where expressions of g_β are given from [2] in Appendix B of [13] and $\bar{\theta}$ given by

$$\begin{cases} \bar{\theta} = \theta & if\ \theta \le \pi\ \ (y' \ge 0) \\ \bar{\theta} = 2\pi - \theta & if\ \theta > \pi\ \ (y' < 0) \end{cases}. \tag{5}$$

$\boldsymbol{d}_{\boldsymbol{\beta}}$ is the polarization vector of the scattered wave, and Γ is the steepest descent contour pictured in Fig. 2. The diffraction angle Ω_β is related to the incidence angle Ω_α by the law of edge diffraction:

$$k_\beta\cos\Omega_\beta = k_\alpha\cos\Omega_\alpha. \tag{6}$$

An asymptotic evaluation of (3) which utilizes the steepest descent method leads to the GTD diffracted field [2]

$$\boldsymbol{u}_\beta^\alpha(\mathbf{x}, \Omega_\alpha, \theta_\alpha) = u^\alpha\big(\mathbf{x}_\beta^\alpha\big)\frac{e^{ik_\beta s'_\beta}}{\sqrt{k_\beta s'_\beta}} D_\beta^\alpha(\Omega_\alpha, \theta_\alpha, \theta)\, \boldsymbol{d}_{\boldsymbol{\beta}}\big(\Omega_\beta, \theta\big), \tag{7}$$

with the diffraction coefficient

$$D_\beta^\alpha(\Omega_\alpha, \theta_\alpha, \theta) = \frac{e^{i\frac{\pi}{4}}}{\sqrt{2\pi}} k_\beta^2 \Psi_\beta(\bar{\theta}, \Omega_\alpha, \theta_\alpha)|\sin\theta|, \tag{8}$$

$s'_\beta = r'/\sin\Omega_\beta$, $r' = (x'^2 + y'^2)^{1/2}$, $\mathbf{x}_\beta^\alpha = (0, 0, z' - s'_\beta\cos\Omega_\beta)$ - the diffraction point on the diffracting edge (the single ray satisfying the law of edge diffraction and reaching $\mathbf{x}$ emanates from $\mathbf{x}_\beta^\alpha$) and $\boldsymbol{u}^{\boldsymbol{\alpha}}\big(\mathbf{x}_{\boldsymbol{\beta}}^{\boldsymbol{\alpha}}\big) = \mathrm{u}^\alpha\big(\mathrm{x}_\beta^\alpha\big)\cdot\mathbf{d}^\alpha$.

Implementing the procedure described in [4], the incremental field $\boldsymbol{F}_\beta(Q_l, \mathbf{x})$ is the field $\boldsymbol{F}_\beta(z' = 0, \mathbf{x})$ radiated by the diffraction point Q_l treated as lying on the edge of the tangential half-plane.

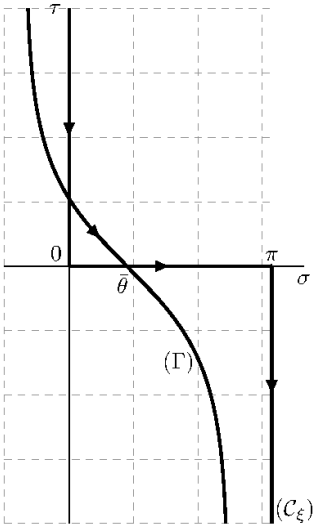

Fig. 2. Integration contours Γ and $\mathcal{C}_\xi$ in the complex plane $\sigma + i\tau$.

It is then assumed that the field diffracted by a half-plane edge is the sum of incremental fields emitted by all diffraction points along the infinite edge:

$$\boldsymbol{u}_\beta^\alpha(\mathbf{x}, \Omega_\alpha, \theta_\alpha) = \int_{-\infty}^{+\infty} \boldsymbol{F}_\beta(z', \mathbf{x}) e^{ik_\alpha z' \cos\Omega_\alpha} dz' \,. \quad (9)$$

Using notation $\xi = \Omega_\alpha$, the inverse Fourier transform gives

$$\boldsymbol{F}_\beta(z', \mathbf{x}) = \frac{k_\alpha}{2\pi} \int_{\mathcal{C}_\xi} \boldsymbol{u}_\beta^\alpha(\mathbf{x}, \xi, \theta_\alpha) \sin\xi \, e^{-ik_\alpha z' \cos\xi} d\xi. \quad (10)$$

The contour $\mathcal{C}_\xi$ in the $\xi = \sigma + i\tau$ plane is shown in Fig. 2. Thus, at any arbitrary observation point, the incremental contribution from Q_l to the diffracted field is

$$\boldsymbol{F}_\beta(Q_l, \mathbf{x}) = \boldsymbol{F}_\beta(z' = 0, \mathbf{x}) = \frac{k_\alpha}{2\pi} u^\alpha(Q_l) \int_{\mathcal{C}_\xi} \boldsymbol{u}_\beta^\alpha(\mathbf{x}, \xi, \theta_\alpha) \sin\xi \; d\xi. \quad (11)$$

Note that the incident field in this local Cartesian coordinate is $u^\alpha(Q_l) = 1$ and is therefore independent of ξ and thus can be taken outside the integral sign. Replacing $\boldsymbol{u}_\beta^\alpha(\mathbf{x}, \xi, \theta_\alpha)$ in (11) by its expression (3), the incremental field $\boldsymbol{F}_\beta(Q_l, \mathbf{x})$ becomes

$$\boldsymbol{F}_\beta(Q_l, \mathbf{x}) = i \frac{\kappa_\beta k_\alpha}{4\pi^2} u^\alpha(Q_l) \int_{\mathcal{C}_\xi} \int_\Gamma q_\beta(\xi) \, \Psi_\beta(\lambda, \xi, \theta_\alpha) \; \sin\lambda \sin\xi \; \boldsymbol{d}_\beta(\xi, \lambda) e^{ig(\lambda,\xi)} \, d\lambda \, d\xi \quad (12)$$

with $g(\lambda, \xi) = k_\beta \left[r' \sin\Omega_\beta(\xi) \cos(\lambda - \bar{\theta}) + z' \cos\Omega_\beta(\xi) \right]$. The angle Ω_β is related to ξ by the law of edge diffraction $k_\beta \cos\Omega_\beta(\boldsymbol{\xi}) = k_\alpha . \cos\boldsymbol{\xi}$. Therefore the phase function in (12) can be written as

$$g(\lambda, \xi) = s' \left[\sin\phi \cos\left(k_\beta^2 - k_\alpha^2 \cos^2\xi \right)^{1/2} + k_\alpha \cos\phi \cos\xi \right], \quad (13)$$

with s' the distance between the observation point and the diffraction point Q_l. Integral (12) has two stationary phase points: $(\lambda_0, \xi_0) = \left(\bar{\theta}, \arccos\left(\frac{k_\beta}{k_\alpha} \cos\phi \right) \right)$ and $(\bar{\theta}, 0)$. (14)

The second phase stationary point corresponds to grazing incidence. In this paper, we study the contribution of the first stationary phase point alone. The obtained results are therefore not valid for any grazing incidence. Applying the steepest descent method to the double integral (12) leads to the following high frequency approximation of the incremental field (see Appendix or [13] for details):

$$\boldsymbol{F}_\beta(Q_l, \mathbf{x}) = \frac{1}{\sqrt{2\pi i}} \sin\phi \; D_\beta^\alpha(\Omega_\alpha(\phi), \theta_\alpha, \theta) \; \boldsymbol{d}_\beta(\phi, \theta) \frac{e^{ik_\beta s'}}{s'}, \quad (15)$$

$$\text{with } \Omega_\alpha(\phi) = \arccos\left(\frac{k_\beta}{k_\alpha} \cos\phi \right). \quad (16)$$

This asymptote of the incremental field, which is valid in the far field zone $k_\beta s' \gg 1$ is a spherical wave weighted by a scattering coefficient. Thus, each point on the defect contour points acts as a fictitious source of spherical wave.

Note that if the contour $\mathcal{L}$ is a straight line (the crack is a half-plane), then substituting (15) into (2), the diffracted field is

$$\boldsymbol{v}_\beta^\alpha(\mathbf{x}) = \int_{-\infty}^{\infty} u^\alpha(Q_l) \frac{\sin\phi(l)}{\sqrt{2\pi i}} D_\beta^\alpha(\Omega_\alpha(\phi(l)), \theta_\alpha, \theta) \frac{e^{ik_\beta s'}}{s'} \boldsymbol{d}_\beta(\phi, \theta) \, dl. \quad (17)$$

In the global Cartesian coordinate system $\{O, \boldsymbol{e}_x = e_x', \boldsymbol{e}_y = e_y', \boldsymbol{e}_z = e_z'\}$ the diffraction point is $Q_l(0,0,l)$. The corresponding phase stationary point l_s is the z-coordinate of the diffraction point on the contour. At this stationary point, $\phi(l_s) = \Omega_\beta$, $s'(l_s) = s'_\beta$ and the phase stationary point contribution to (17) is

$$\boldsymbol{v}_\beta^\alpha(\mathbf{x}) = \mathrm{e}^{ik_\alpha l_s \cos\Omega_\alpha} D_\beta^\alpha(\Omega_\alpha, \theta_\alpha, \theta) \; \boldsymbol{d}_\beta(\Omega_\beta, \theta) \frac{e^{ik_\beta s'_\beta}}{\sqrt{k_\beta s'_\beta}}. \quad (18)$$

ITD gives thus the GTD solution (7) for infinite straight edges.

B. The Huygens method

According to Huygens, when impacted by an incident plane wave, each point on an obstacle serves as the source of a spherical secondary wavelet with the same frequency as the primary wave. The amplitude at any point is the superposition of these wavelets. This theory gives a simple qualitative description of diffraction but needs to be adapted to provide a good agreement with more exact scattering formulations (such as GTD). Therefore, in our Huygens method, we postulate an ansatz in which the amplitude of the scattered field at an observation point is obtained by integrating the spherical waves contributions from the points along the edge and by weighting each contribution by a directivity factor (henceforth named K):

$$\boldsymbol{v}_\beta^\alpha(\mathbf{x}) = \int_{\mathcal{L}} \boldsymbol{K} \, u^\alpha(Q_l) \frac{e^{ik_\beta s'}}{s'} \, dl, \quad (19)$$

where $\mathcal{L}$ is the crack contour; dl is the length of an elementary arc along the contour $\mathcal{L}$. To determine the unknown $\boldsymbol{K}$ vector in (19), we again use Huygens' principle: the latter tells us that the scattered wavefront from an infinite straight edge is the envelope of the secondary spherical waves and is thus cylindrical or conical in the field far from the flaw as predicted by GTD. To mathematically transform the sum of spherical waves of our Huygens proposed integral into a cylindrical or

conical wave form, we apply below the stationary phase method to Huygens' integral for a straight infinite edge and the obtained far-field approximation is identified to the GTD one to fix the K coefficient.

If the contour $\mathcal{L}$ is a straight segment with ends a and b, the angles of incidence Ω_α and θ_α are the same at any discretization points on the diffracting edge. In the frame $\{O, \boldsymbol{e}_x, \boldsymbol{e}_y, \boldsymbol{e}_z\}$, the distance between the diffraction point $Q_l = (0,0,l)$ on the contour $\mathcal{L}$ and an observation point $\mathbf{x} = (\mathrm{x},\mathrm{y},\mathrm{z}) = (x', y', z' + l)$ is $s' = \left[(z-l)^2 + r'^2\right]^{1/2}$ with $r' = \left(x'^2 + y'^2\right)^{1/2}$. Using the law of edge diffraction (6) the phase function of diffracted field (19) can be written as

$$q(l) = \sqrt{(z-l)^2 + r'^2} + l\cos\Omega_\beta. \tag{20}$$

The stationary phase point is the edge diffraction point $(0,0,l_s)$ with $l_s = z - r'/\tan\Omega_\beta$. (21)

Therefore in the far-field $\left(k_\beta r' \gg 1\right)$, the diffracted field (19) can be approximated by the phase stationary method:

$$\boldsymbol{v}_\beta^\alpha(\mathbf{x}) = H(l_s - a)H(b - l_s)\, A\, \boldsymbol{K} e^{i\frac{\pi}{4}} \frac{\sqrt{2\pi}}{\sin\Omega_\beta} \frac{e^{i\left(k_\alpha l_s \cos\Omega_\alpha + k_\beta s'_\beta\right)}}{\sqrt{k_\beta s'_\beta}} \tag{22}$$

when the phase stationary point is far from the edge extremities a and b. H is the Heaviside function. The coefficients vector K can be chosen to be

$$\boldsymbol{K} = \frac{\sin\Omega_\beta}{\sqrt{2i\pi}}\; D_\beta^\alpha(\Omega_\alpha, \theta_\alpha, \theta)\boldsymbol{d}_\beta\left(\Omega_\beta, \theta\right), \tag{23}$$

so that for an infinite straight edge $(a \to -\infty, b \to \infty)$ the stationary point contribution gives the GTD diffracted field (7). The formulation of Huygens method (19) has similitudes with Eq. (45) of the paper [11]. But this cited equation was simply a step of calculation in [11] and led to no modelling application. Moreover this equation has been established only for an elliptic crack and for compressional waves. By contrast, the Huygens method proposed here can be applied for any crack shape and also for shear waves.

Finally, incremental fields in the ITD and Huygens models can both be represented using the K function by

$$\boldsymbol{F}_\beta(Q_l, \mathrm{x})\big|_{\mathrm{ITD}} = \frac{e^{ik_\beta s'}}{s'}\, K(\Phi(l))\,, \tag{24}$$

$$\boldsymbol{F}_\beta(Q_l, \mathrm{x})\big|_{\mathrm{Huygens}} = \frac{e^{ik_\beta s'}}{s'}\, K\left(\Omega_\beta\right), \tag{25}$$

$$\text{with } \boldsymbol{K}(\zeta) = \frac{\sin\zeta}{\sqrt{2\pi i}} D_\beta^\alpha(\Omega_\alpha(\zeta), \theta_\alpha, \theta)\boldsymbol{d}_\beta(\zeta, \theta). \tag{26}$$

The Huygens formula (25) differs from the ITD formula (24) by the argument ζ of the coefficient $K(\zeta)$. In ITD, ζ is the angle ϕ characterizing the ray issuing from an arbitrary discretization point to the observation point, whereas in the Huygens method it is the diffraction angle Ω_β. Consequently, ITD is parametrized by the local angle ϕ whereas the Huygens method is parametrized by the incident angle Ω_α according to (6). Both methods add endpoints contributions to the classical edge contribution. Even if endpoints probably radiate differently from other points inside the edge segment, the ITD and Huygens models lead to a more physical description than GTD's one [see Fig. 3 a) and 4a) in next section].

III. Results

A. Implementation

For both Huygens and ITD models, the diffracted field is then computed using equation (2) (and (24)-(26) for ITD, (25)-(26) for Huygens), where the integration along the edge $\mathcal{L}$ is approached numerically by a discrete sum. For the case studied here of an incident plane wave, the GTD diffraction coefficient and scattered polarization are the same for all meshed edge points for Huygens computations (see (25)) whereas they vary along the edge for ITD (see (24) depending on $\Phi(l)$). Huygens is consequently much less time consuming than ITD.

B. Numerical Tests

The ITD and Huygens models have been subject to two different kinds of numerical tests. In both tests the longitudinal/transversal speeds and frequency of the incident wave are respectively $c_L = 5900\, m/s, c_T = 3230 m/s$ and 1MHz.

The first test is a comparison to GTD. The numerical tests involve here a longitudinal oblique ($\Omega_{\alpha=L} = 60°, \theta_{\alpha=L} = 60°$) incident wave and both longitudinal (Fig. 3) and transversal (Fig. 4) diffracted waves from a finite straight edge. The frame center O is taken as the center of a 40mm long crack edge. The observation points are chosen to lie in the plane (e'_y, e'_z) normal to the crack plane and containing the crack edge (see Fig. 1): $\theta = 90°$ or $\theta = 270°$. There is no shadow boundary of the incident or reflected fields (divergence of the GTD diffraction coefficient) in this observation plane since, for example, for P scattered waves, $\theta \neq \theta_\alpha$ and $\theta \neq 2\pi - \theta_\alpha$.

GTD is a ray method. Given an observation point, the diffraction point on the edge can be found, which gives rise to a diffracted ray satisfying the law of edge diffraction and reaching this observation point. The diffracted field amplitude is then evaluated using the GTD formula (7). The classical GTD produces a discontinuity at the shadow boundaries emanating from the edge endpoints [see Figs. 3a) and 4a)]. Unlike GTD, the Huygens model involves summing up the wavelets generated by the fictitious sources on the edge. Therefore, in this model (and also in ITD) the edge endpoints contribute to the diffracted field, making it continuous [see Fig. 3b) and 4b)]. Since GTD is discontinuous at the shadow boundary of the edge endpoints but Huygens (or ITD) is continuous, the difference between GTD and Huygens (or ITD) solutions [see Fig. 3 d)] is discontinuous and behaves as a sign function. The appearance of the sign function can be mathematically shown by calculating the asymptotic uniform contribution of coalescing extremity points and stationary phase points in the Huygens' integral using a method proposed by Borovikov [14]. Extremity points then correspond to the waves diffracted by the edge endpoints and stationary phase points to waves diffracted from the edge itself. This difference highlights the Huygens spherical waves emitted by endpoints which interfere with each other [see Figs. 3 b) and d)] and render the Huygens field continuous at endpoints shadow boundaries contrary to GTD. On these figures, the difference between GTD and Huygens (or ITD)

increases near the edge, y~ 0 mm. That does not matter because near the edge, neither GTD nor Huygens (nor ITD) provide a valid result since they are far-field approximations. In the edge near field, Huygens is closer to GTD than ITD and in far field, Huygens and ITD are similar. In near field, the ITD coefficient given by (24) and depending of the local angle ϕ varies more rapidly than the Huygens one from a diffraction point to another and the summation of secondary sources is more destructive. These observations are more pronounced for the mode-converted transversal diffracted wave in Fig. 4.

Echoes from the endpoints contributions obtained with ITD and Huygens models are not exact since they still rely on canonical GTD solutions (infinite half-plane or wedge). But these incremental methods produce a spatially continuous field and consequently a more physical representation than GTD one's.

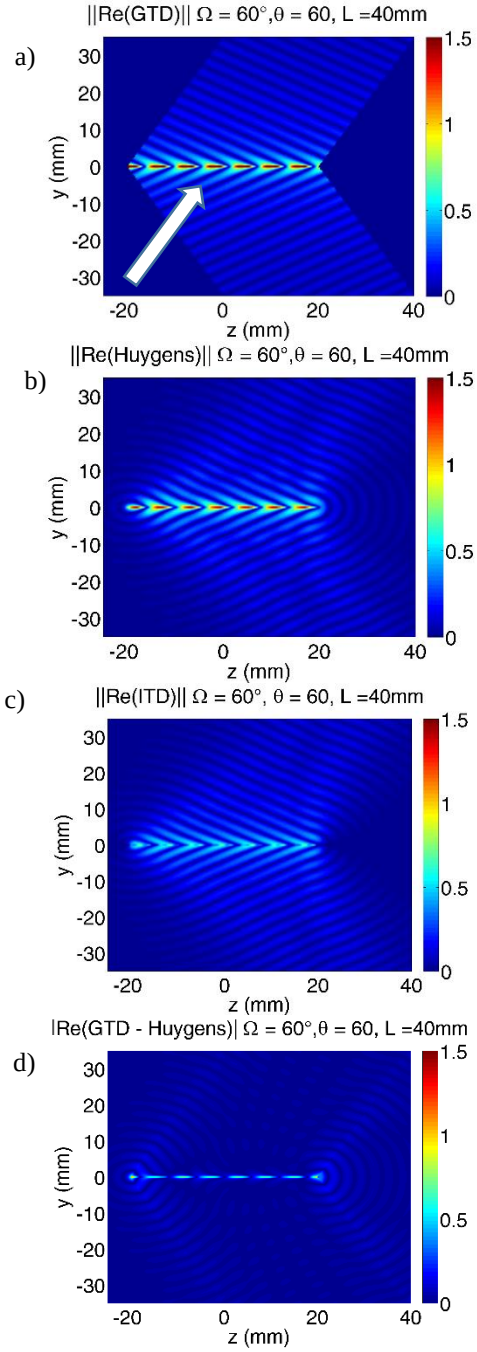

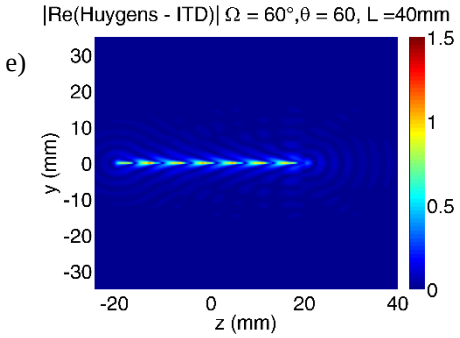

Fig. 3. Diffraction of an oblique incident longitudinal wave (white arrow, $\Omega_{\alpha} = 60°, \theta_{\alpha=L} = 60°$) by a planar 40 mm long crack, observed in the plane normal to the crack and containing the crack edge. Results for the longitudinal diffracted wave, normalized by the incident amplitude: real parts of GTD a), Huygens b) and ITD c) solutions. Absolute difference between real parts of: d) Huygens and GTD solutions; e) Huygens and ITD solutions.

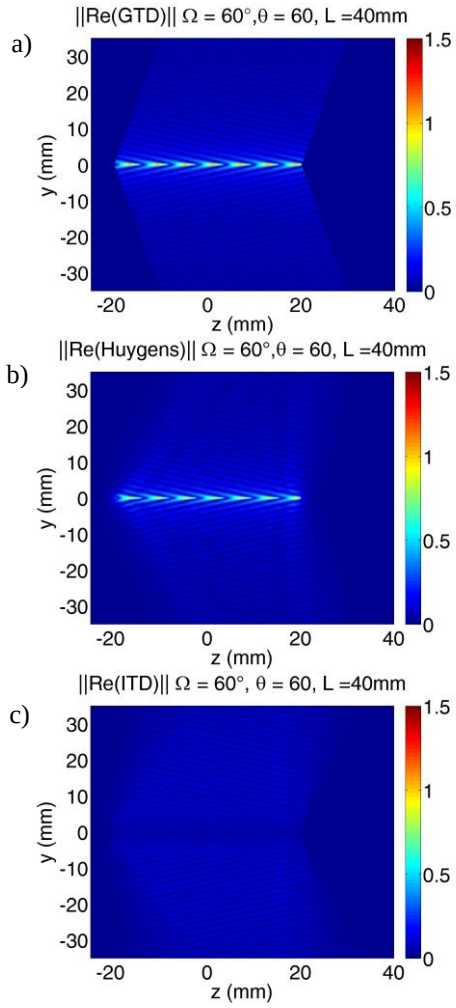

Fig. 4. Results in the configuration of Fig.3 for the transversal diffracted wave: a),b) and c) with the same meaning as in Fig. 3.

It has been numerically checked that as the edge length increases, the Huygens and ITD models both converge to GTD. The second test is a comparison between GTD, Huygens, ITD and a Finite Differences (FD) numerical model [15]. An edge of length L (see Fig. 5. a) is impinged by an incident longitudinal plane wave. The amplitude (absolute value) of the

longitudinal edge diffracted field is plotted for two flaw lengths L versus the observation angle ϕ of observation points located in the plane (e'_y, e'_z) at a distance $R = 30mm$ of 5 wavelengths from the flaw center. Since this observation plane is in the shadow boundary of the incident $(\theta = \theta_\alpha)$ or reflected $(\theta = 2\pi - \theta_\alpha)$ fields, the analytical models are all combined with the Uniform Theory of Diffraction (UTD) [16]: the UTD diffraction coefficient is then finite contrary to the GTD one. As in Figs. 3 and 4, the GTD diffracted field is discontinuous at the shadow boundaries (angles $\phi_1, \ldots, \phi_4$ in Fig. 5.a) emanating from the edge endpoints. ITD and Huygens methods give generally accurate and similar results for observation points for which there exists a GTD diffraction point on the edge $(\phi_1 < \phi < \phi_2$ and $(\phi_3 < \phi < \phi_4)$ and even around these regions. Huygens has a more physical behavior than ITD for small edge lengths for regions surrounding $\phi = 0$ and $\phi = 180°$ (where ITD vanishes due to destructive interferences as shown also in Figs. 3.c and 4.c for y=0).

C. *Experimental validation*

The echoes diffracted by the top tip of a $40\,mm$ long and $10\,mm$ high planar notch breaking the backwall of a ferritic steel component have been simulated by the two previous incremental methods and compared to both experimental and numerical results. This comparison briefly presented in section 2 of [17] is reproduced here to make the paper self-consistent since the theory of incremental methods is completely detailed here[1]; the results simulated by a Huygens/2.5D GTD model and by a hybrid numerical model are shown here in addition. The objective of this experimental validation is to evaluate the ability of the developed incremental models to simulate the echo amplitude of a defect edge of finite extent.

The diffraction echoes have been measured in a TOFD (Time Of Flight Diffraction) contact configuration (see Fig. 6) using two $6.35\,mm$ diameter, single element, Plexiglas wedge type transducers emitting compressional P-waves at 45° incidence and $2.25\,MHz$. The flaw skew angle (angle between the top edge of the notch and Y-axis, see Fig. 6) has been varied from 0° to 70° by rotating the specimen around the Z-axis. S-waves are generated in the specimen but the main and first arrival echo from the specimen bulk is due to incident P-wave->scattered P-wave diffraction from the top crack edge. To compute the ultrasonic response of flaws, we have used a reciprocity-based measurement model whose principles and abilities are described in more details in [18]. In order to avoid modelling of the pulser, cabling, electroacoustic transduction and electronics at emission/reception, this model requires as input the experimental signal obtained by a calibration measurement on a reference flaw. A side-drilled hole of 2mm diameter and 40mm length (in red in Fig. 6) has been used for calibration. Our first measurement model [18] applied plane-wave approximations to the ultrasonic fields at each flaw mesh point in order to calculate diffraction coefficients. It yields satisfying results in most usual configurations but can lead to inaccuracies in unfavorable cases, such as for wide probe apertures, outside of the focal region, or for beam-splitting or distortion due to irregular geometries.

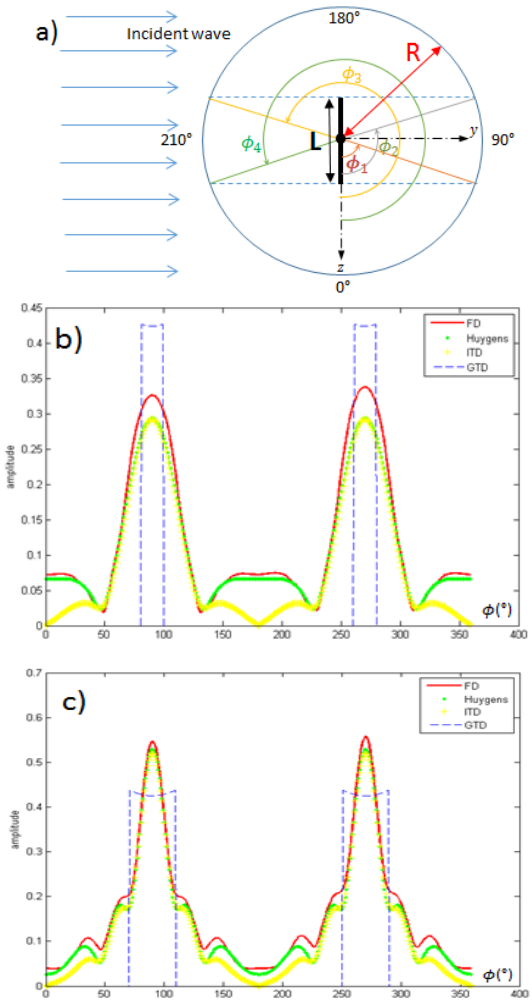

Fig. 5. a) An edge of length L impinged by an incident longitudinal plane wave. Longitudinal edge diffracted field simulated by different models: b) L=10mm; c) L=20mm.

A new ray based model [19] describes the ultrasonic field as a sum of rays emanating from meshed points of the transducer surface and applies the plane-wave approximation to each ray instead of the entire mean field. It can significantly improve the accuracy of echo computations since the GTD diffraction coefficient is calculated at each mesh flaw contour point for each pair of incident and diffracted rays instead of being calculated only once. In Fig. 7 the maximal amplitude of the P->P echo signal is plotted for both experimental and simulated results. In the current configuration, plane wave approximation and the ray based model lead to quasi identical results since the flaw is far from the probes and the maximal flaw echo amplitude is obtained for the flaw edge location on the probes focal axis. The ray based model results are slightly closer to those of a hybrid FEM model [20] (mixing a ray model for beam calculation and spectral finite elements for flaw scattering modelling).

[1] Only the main results are presented in [17] (reusing portions from [17] in other works is allowed). The current article is cited in [17] under the submitted reference [10] to refer to the theory of the incremental models.

The Huygens/GTD and ITD/GTD results are similar and close to experiments even for large skews with a maximal difference of 2 dB, which is of order of measurement errors [21]. Huygens/2.5D GTD model breaks down for skew angles greater than 30°. Therefore the experimental validation of both ITD and Huygens methods in a 3D configuration and with a finite size flaw has been successful.

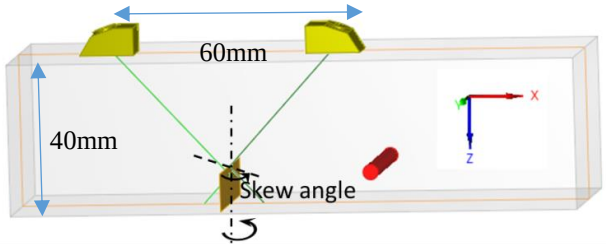

Fig. 6. TOFD inspection used for experimental validation.

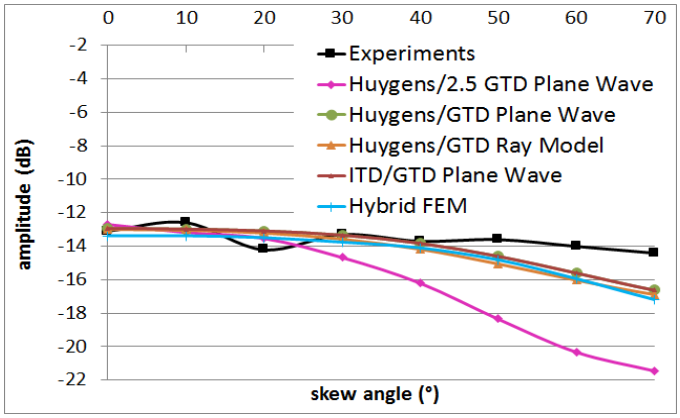

Fig. 7. Echo amplitude diffracted by the top tip.

IV. Conclusion

Two incremental methods have been proposed for use in elastodynamics to predict diffraction from edges of a finite length. Both methods are based on the edge integral approach. For the plane wave incident on a half-plane both methods reproduce the canonical GTD solution, but, unlike the latter they lead to a field which is spatially continuous notably at the shadow boundaries due to edge endpoints. The methods have been tested numerically and validated against experiments for a backwall planar crack. Such methods can be combined with the recently developed elastodynamic corrections to GTD, which are valid in the vicinity of shadow boundaries, the Physical Theory of Diffraction (PTD) [12] and the Uniform Theory of Diffraction (UTD) [16] or in the vicinity of critical angles [22].

Appendix

Let us show how to evaluate the double integral (12). Denoting it by I it can be written as

$$I = \int_{\Gamma}\int_{\mathcal{C}_\xi} \boldsymbol{A}(\lambda,\xi)\ \mathrm{e}^{-s' f(\lambda,\xi)}\ d\lambda d\xi, \tag{27}$$

with

$$\boldsymbol{A}(\lambda,\xi) = \frac{i(\kappa_\beta k_\alpha)}{4\pi^2} u^\alpha(Q_l)\ q_\beta(\xi)\Psi_\beta(\lambda,\xi,\theta_\alpha)\sin\lambda\ \sin\xi\ \boldsymbol{d_\beta}(\xi,\lambda) \tag{28}$$

and

$$f(\lambda,\xi) = -i\left[\sin\phi\cos(\lambda-\bar{\theta})\ \left(k_\beta^2 - k_\alpha^2\cos^2\xi\right)^{\frac{1}{2}} + k_\alpha\cos\phi\cos\xi\right] \tag{29}$$

where (13) was used. Integral I can be approximated using the steepest descent method [14] to give

$$I \sim \frac{2\pi}{s'}\frac{A(\lambda_s,\xi_s)}{\sqrt{\det H(\lambda_s,\xi_s)}} e^{-s' f(\lambda_s,\xi_s)} \tag{30}$$

where H is the Hessian matrix. All the functions above are evaluated at the phase stationary point at which we have

$$0 = \partial_\lambda f = i\left[\sin\phi\ \sin(\lambda-\bar{\theta})\left(k_\beta^2 - k_\alpha^2\, cos^2\,\xi\right)^{\frac{1}{2}}\right]; \tag{31}$$

$$0 = \partial_\xi f = -i\left[k_\alpha^2\sin\phi\cos(\lambda-\bar{\theta})\sin\xi\cos\xi\left(k_\beta^2 - k_\alpha^2\cos^2\xi\right)^{-\frac{1}{2}} - k_\alpha\cos\phi\ \sin\xi\right]. \tag{32}$$

Therefore the stationary point is $\lambda_s = \bar{\theta},\ \ \xi_s = 0$

$$\text{or } \cos\xi_s = \frac{k_\beta}{k_\alpha}\cos\phi \tag{33}$$

and according to (16), $\xi_s = \Omega_\alpha(\phi)$. We have also

$$\partial^2_{\lambda\lambda} f = i\left[\sin\phi\ \cos(\lambda-\bar{\theta})\left(k_\beta^2 - k_\alpha^2\cos^2\xi\right)^{\frac{1}{2}}\right], \tag{34}$$

$$i\,\partial^2_{\xi\xi} f = k_\alpha^2\sin\phi\cos(\lambda-\bar{\theta})\left(k_\beta^2 - k_\alpha^2\cos^2\xi\right)^{-\frac{1}{2}} \tag{35}$$

$$\left[\cos^2\xi - \sin^2\xi - \frac{k_\alpha^2\sin^2\xi\cos^2\xi}{k_\beta^2 - k_\alpha^2\cos^2\xi}\right] - k_\alpha\cos\phi\ \cos\xi\,;$$

$$\partial^2_{\lambda\xi} f = \partial^2_{\xi\lambda}(g) = i\left[k_\alpha^2\sin\phi\sin(\lambda-\bar{\theta})\sin\xi\cos\xi\left(k_\beta^2 - k_\alpha^2\cos^2\xi\right)^{-\frac{1}{2}}\right]. \tag{36}$$

Finally, at the diffraction point (λ_s,ξ_s),

$$\partial^2_{\lambda\lambda} f\big|_{(\lambda_s,\xi_s)} = ik_\beta\sin^2\phi, \tag{37}$$

$$\partial^2_{\xi\xi} f\big|_{(\lambda_s,\xi_s)} = i\frac{k_\alpha^2 - k_\beta^2\cos^2\phi}{k_\beta\sin^2\phi}, \tag{38}$$

$$\partial^2_{\lambda\xi}(g)\big|_{(\lambda_s,\xi_s)} = 0. \tag{39}$$

Using (39) - (41), the Hessian matrix at the stationary point is

$$H(\lambda_s,\xi_s) = \begin{bmatrix} ik_\beta\sin^2\phi & 0 \\ 0 & i\frac{k_\alpha^2 - k_\beta^2\cos^2\phi}{k_\beta\sin^2\phi} \end{bmatrix}. \tag{40}$$

and $\det[H(\lambda_s,\xi_s)] = -k_\alpha^2\sin^2\Omega_\alpha(\phi)$. (41)

Since $f(\lambda_s,\xi_s) = -ik_\beta$ and (42)

$$\boldsymbol{A}(\lambda_s,\xi_s) = \frac{i(\kappa_\beta k_\alpha)}{4\pi^2} u^\alpha(Q_l)\ q_\beta\big(\Omega_\alpha(\phi)\big)\Psi_\beta(\bar{\theta},\Omega_\alpha(\phi),\theta_\alpha)$$
$$|\sin\theta|\ \sin\Omega_\alpha(\phi)\ \boldsymbol{d_\beta}(\phi,\theta), \tag{43}$$

substituting the above expressions into (3), we get

$$I \sim \frac{1}{2\pi}\frac{e^{ik_\beta s'}}{s'}\sin\phi\, u^\alpha(Q_l)k_\beta^2\Psi_\beta(\bar{\theta},\Omega_\alpha(\phi),\theta_\alpha)|\sin\theta|\boldsymbol{d_\beta}(\phi,\theta) \tag{44}$$

and according to (8)

$$I \sim \frac{\sin\phi}{\sqrt{2i\pi}} u^\alpha(Q_l)\frac{e^{ik_\beta s'}}{s'} D_\beta^\alpha(\Omega_\alpha(\phi),\theta_\alpha,\theta)\boldsymbol{d_\beta}(\phi,\theta) \tag{45}$$

REFERENCES

[1] J. B. Keller, "Geometrical theory of diffraction," *J Opt Soc Am*, vol. 52, pp. 116–130, 1962.

[2] J. D. Achenbach, A. K. Gautesen, and H. McMaken, *Rays methods for waves in elastic solids*. Pitman, 1982.

[3] D. Bouche, F. Molinet, and R. Mittra, *Asymptotic methods in electromagnetics*. Springer, 1997.

[4] R. Tiberio and S. Maci, "An incremental theory of diffraction: scalar formulation," *IEEE Trans. Antennas Propag.*, vol. 42, no. 5, pp. 600–612, May 1994.

[5] R. Tiberio, S. Maci, and A. Toccafondi, "An incremental theory of diffraction: Electromagnetic formulation," *IEEE Trans Ant Prop*, vol. 43, no. 1, pp. 87–96, Jan. 1995.

[6] R. Tiberio, A. Toccafondi, A. Polemi, and S. Maci, "Incremental theory of diffraction: a new-improved formulation," *IEEE Trans. Antennas Propag.*, vol. 52, no. 9, pp. 2234–2243, Sep. 2004.

[7] A. D. Yaghjian, "Incremental length diffraction coefficients for arbitrary cylindrical scatterers," *IEEE Trans. Antennas Propag.*, vol. 49, no. 7, pp. 1025–1032, Jul. 2001.

[8] A. Michaeli, "Elimination of infinities in Equivalent Edge Currents, Part II: Physical Optics Components," *IEEE Trans Antennas Propagat*, vol. 34, no. 8, pp. 1034–1037, 1986.

[9] R. G. Kouyoumjian and P. H. Pathak, "A Uniform Geometrical Theory of Diffraction for an Edge in a Perfectly Conducting Surface," *Proc. IEEE*, vol. 62, no. 11, pp. 1448–1461, 1974.

[10] A. J. Dawson, J. E. Michaels, J. W. Kummer, and T. E. Michaels, "Quantification of Shear Wave Scattering From Far-Surface Defects via Ultrasonic Wavefield Measurements," *IEEE Trans. Ultrason. Ferroelectr. Freq. Control*, vol. 64, no. 3, pp. 590–601, Mar. 2017.

[11] L. J. Fradkin and R. Stacey, "The high-frequency description of scatter of a plane compressional wave by an elliptic crack," *Ultrasonics*, vol. 50, no. 4, pp. 529–538, 2010.

[12] V. Zernov, L. Fradkin, and M. Darmon, "A refinement of the Kirchhoff approximation to the scattered elastic fields," *Ultrasonics*, vol. 52, no. 7, pp. 830–835, 2012.

[13] A. K. Djakou, "Modeling of diffraction effects for specimen echoes simulations in ultrasonic Non-Destructive Testing (NDT)," phdthesis, Université du Maine, 2016.

[14] V. A. Borovikov, *Uniform Stationary Phase Method*. London, UK: IEE, 1994.

[15] E. Bossy, M. Talmant, and P. Laugier, "Three-dimensional simulations of ultrasonic axial transmission velocity measurement on cortical bone models," *J. Acoust. Soc. Am.*, vol. 115, no. 5, pp. 2314–2324, Apr. 2004.

[16] A. K. Djakou, M. Darmon, L. Fradkin, and C. Potel, "The Uniform geometrical Theory of Diffraction for elastodynamics: Plane wave scattering from a half-plane," *J. Acoust. Soc. Am.*, vol. 138, no. 5, pp. 3272–3281, Nov. 2015.

[17] A. K. Djakou, M. Darmon, and C. Potel, "Elastodynamic Models for Extending GTD to Penumbra and Finite Size Scatterers," *Phys. Procedia*, vol. 70, pp. 545–549, 2015.

[18] M. Darmon and S. Chatillon, "Main features of a complete ultrasonic measurement model - Formal aspects of modeling of both transducers radiation and ultrasonic flaws responses," *Open J. Acoust.*, vol. 3A, 2013.

[19] V. Dorval, N. Leymarie, and S. Chatillon, "Improved semi-analytical simulation of UT inspections using a ray-based decomposition of the incident fields," in *AIP Conference Proceedings*, 2016, vol. 1706, p. 070002.

[20] A. Imperiale, S. Chatillon, M. Darmon, N. Leymarie, and E. Demaldent, "UT simulation using a fully automated 3D hybrid model: Application to planar backwall breaking defects inspection," *AIP Conf. Proc.*, vol. 1949, no. 1, p. 050004, Apr. 2018.

[21] R. Raillon-Picot, G. Toullelan, M. Darmon, and S. Lonné, "Experimental study for the validation of CIVA predictions in TOFD inspections," in *10th International Conference on NDE in Relation to Structural Integrity for Nuclear and Pressurized Components, Cannes, Oct 2013*, 2013.

[22] L. J. Fradkin, M. Darmon, S. Chatillon, and P. Calmon, "A semi-numerical model for near-critical angle scattering," *J. Acoust. Soc. Am.*, vol. 139, no. 1, pp. 141–150, Jan. 2016.

Michel Darmon received the diploma of engineering at ESPCI ParisTech, Paris, France, in 1999 and a Ph.D. degree in physical acoustics from the University of Paris VII in 2002 for modeling the ultrasonic response of solid inclusions, carried out at CEA and ArcelorMittal. He obtained in 2015 the Habilitation to supervise research (Univ. Paris-Sud XI). He's an expert of the French Atomic Energy Commission (CEA/LIST). His research activity is in ultrasonic modeling notably in flaws scattering and wave propagation in complex media.

Audrey Kamta Djakou received the French engineer degree from ENSEIRB-MATMECA, Bordeaux in 2013 and the Ph.D. degree in acoustics in 2016 at the Maine University, France. Her PhD works have been carried out at CEA/LIST about NDT simulation and notably waves diffraction.

Samar Chehade received a French engineering degree from ENSTA ParisTech in 2016 and is a PhD candidate in acoustics at the Paris-Sud University in France. Her research at CEA/LIST is about NDT simulation and notably acoustic and elastic waves diffraction.

Larissa Fradkin received a Ph.D. in applied mathematics from the Victoria University of Wellington, NZ in 1977. She worked as a research scientist (1977-1984) at the Department of Scientific and Industrial Research, NZ, research associate (1985-1993 at the Department of Applied Mathematics and Theoretical Physics, University of Cambridge, UK and then a Senior Lecturer, Reader and Professor of Electrical Engineering at London South Bank University (1993-2009). Since 2009 she is running a micro company Sound Mathematics Ltd. Her research interests include mathematical modeling of ultrasonic NDT (notably high-frequency phenomena in elastodynamics).

Catherine Potel received a Ph.D. degree in mechanical engineering from the University of Technology of Compiègne (UTC), France, in 1994. She was lecturer at the University of Amiens, France, from 1996 to 2001 and has been a professor of physical acoustics and of mechanics at the University of Le Mans, France, in the Laboratoire d'Acoustique de l'Université du Maine since 2001. Her research is in ultrasonics for nondestructive evaluation and materials characterization, with special interest in propagation in anisotropic multilayered media such as composites and in rough plates.